Chapter 5

Wavelet approximation with finite volume framework

Contents

5.1 Introduction

In this chapter algorithm of the wavelet approximation is combined along with the finite volume technique for solving the partial differential equation. The choice of space of resolution considered in multi resolution framework improves the decomposed solution and the reconstruction phenomena. Extraction of the detailed pattern in the required region of sudden change is achieved. Accuracy of the approach is discussed with decomposed solution in multi resolution framework. Test cases are discussed to validate the approach.

Simplicity of the approach is highlighted which is improved by closely recording the error approximation. The method is compared with already available approaches in literature such as finite volume Godunov approach and exact solution obtained

by method of characteristics. A comparison of proposed approach with Haar, Daubechies and Coiflet wavelet basis is also considered for a better understanding of localized behaviour of the approach. Before discussing our approach the basics of hyperbolicity of the linear systems, shallow water wave equation and finite volume framework are discussed briefly.

Hyperbolicity of the linear system A linear system of the form

$$w_t + Aw_x = 0 \tag{5.1.1}$$

is called hyperbolic if the $m \times m$ matrix A is diagonalizable with real eigenvalues. Here the eigen values are considered as $\lambda^1 \leq \lambda^2 \leq \ldots \leq \lambda^m$.
The matrix is diagonalizable if there is a complex set of eigenvectors i.e. if there are nonzero vectors $r^1, r^2, \ldots, r^m \in R^m$ such that

$$Ar^p = \lambda^p r^p \tag{5.1.2}$$

for $p = 1, 2, \ldots, m$ and these vectors are linearly independent.
The matrix $R = [r^1|r^2|\ldots|r^m]$,
formed by collecting the vectors $r^1, r^2, \ldots, r^m$ together, is nonsingular and has an inverse R^{-1}. Hence,

$$R^{-1}AR = \Lambda \tag{5.1.3}$$

and $A = R\Lambda R^{-1}$

with

$$\Lambda = \begin{bmatrix} \lambda^1 & & & \\ & \lambda^2 & & \\ & & \ddots & \\ & & & \lambda^m \end{bmatrix} \equiv diag(\lambda^1 \leq \lambda^2 \leq \ldots \leq \lambda^m) \tag{5.1.4}$$

Hence A is transformed to diagonal form by similarity transformation. So the linear system can be rewritten as,

$$R^{-1}w_t + R^{-1}ARR^{-1}w_x = 0 \tag{5.1.5}$$

Defining $z(x,t) \equiv R^{-1}w(x,t)$ leads to ,

$$z_t + \Lambda z_x = 0 \tag{5.1.6}$$

Since each Λ is diagonal, this system decouples into m independent advection equations for the components z^p of z :

$$z_t^p + \lambda^p z_x^p = 0 \tag{5.1.7}$$

for $p = 1, 2, \ldots, m$.

Since each of λ^p is real, these advection equations make sense physically and can be used to solve the original system which has solutions represented as waves traveling at the characteristic speeds $\lambda^1 \leq \lambda^2 \leq \ldots \leq \lambda^m$. These values represent the characteristic curves along which information propagates in the decoupled advection

equations as viewed in an analytic solution.

This motivates us to consider the solution assumption to be an approximation of wavelet basis within the cell intervals in FVM. This idea was implemented in the work of Haleem [28] for solving the shallow water equation.

He considered the shallow water wave equations, which are an attempt to model fluid flow in a confined region such as harbors where the depth is relatively small. The unknown parameters were, height $= h(x, y, t)$ above the bottom, $x-$ velocity $= u(x, y, t)$ and $y-$ velocity $= v(x, y, t)$. The governing equations were conservation of mass and conservation of momentum in both the x and y directions.

The conservation matrix form of shallow water wave equation is given by,

Shallow water wave equations

$$U_t + F(U)_x + G(U)_y = 0 \tag{5.1.8}$$

in R^3 where

$$U = \begin{bmatrix} h \\ uh \\ vh \end{bmatrix} \tag{5.1.9}$$

$$F(U) = \begin{bmatrix} uh \\ u^2h + \frac{1}{2}gh^2 \\ uvh \end{bmatrix} \tag{5.1.10}$$

and

$$G(U) = \begin{bmatrix} vh \\ uvh \\ v^2h + \frac{1}{2}gh^2 \end{bmatrix} \tag{5.1.11}$$

The equations are also commonly known as Saint Venant equations, Haleem considered the one dimensional case with source term as,

$$\frac{\partial U}{\partial t} + \frac{\partial F(U)}{\partial x} = S \tag{5.1.12}$$

with

$$U = [h, q]^T, \quad F(U) = [q, \frac{gh^2}{2} + \frac{q^2}{h}]^T \quad and \quad S(U) = [0, -gh(S_0 - S_f)]^T \tag{5.1.13}$$

where t is the time (s), x is space (m) and U, F and S are the vectors containing the conserved variables, the fluxes and the bed source terms, respectively, in which h is the water depth (m), q is the flow rate per unit width ($\frac{m^3}{s.m}$), g is the acceleration gravity ($\frac{m}{s^2}$) and z is the bed elevation (m). For a rectangular channel, S_f in terms of Manning's equations and S_0 have the following expressions

$$\begin{aligned} S_f &= \frac{n^2|q|q}{h^2 R^{\frac{4}{3}}}, \\ S_0 &= \partial_x z \end{aligned} \tag{5.1.14}$$

Finite volume framework The Godunov type finite volume approach considers the division of the domain into uniform non overlapping control volumes, each cell is defined as $I_i = [x_{i-\frac{1}{2}}, x_{i+\frac{1}{2}}]$ having cell size $\delta x = x_{i+\frac{1}{2}} - x_{i-\frac{1}{2}}$ having centre at $\frac{x_{i+\frac{1}{2}} + x_{i-\frac{1}{2}}}{2}$.

Integrating to formulate the integral equation for equation 5.1.12 by integrating over space and then over time domain $t_k = t \quad to \quad t_{k+1} = t + \delta t$, the discrete form is given as,

$$U_i^{t^{k+1}} = U_i^{t^k} - \frac{\delta t}{\delta x_i}(F_{i+\frac{1}{2}}^{t^k} - F_{i-\frac{1}{2}}^{t^k}) + \delta t S_i^{t^k} \tag{5.1.15}$$

where $U_i^{t^k}$ represents the local numerical solution at a time. It is a piecewise constant average representation. $F_{i+\frac{1}{2}}^{t^k}$ represents the flux at cell interface which depends on the choice of flux.

Haleem choose to approximate solution in terms of Haar wavelet and evaluated the equation 5.1.15 as,

$$\begin{aligned} U_{i,j}^{n,t^{k+1}} &= U_{i,j}^{n,t^k} + \delta t L_{i,j}^n \\ with \quad L_{i,j}^{n_i} &= \frac{-2^n\sqrt{2}}{\delta x_i}(F^{Roe}(U_{i-1,j}^{n_{i-1}}, U_{i,j}^{n_i}) + F^{Roe}(U_{i+1,j}^{n_{i+1}}, U_{i,j}^{n_i})) \end{aligned} \tag{5.1.16}$$

where j indicates the resolution chosen for the local cell n. $F^{Roe}(U_{i,j}^{n_i})$ indicates the flux chosen to be Roe.

In our study we have considered different numerical fluxes, for the Burger equations with wavelet families which is an extension to Haleems work where he restricted to shallow water problem with Haar wavelets only.

We have also analyzed the experimental order of accuracy for our proposed approach to justify its accuracy.

Solution of Burger inviscid equation is formulated using the proposed wavelet based finite volume approach in this chapter which is compared with the classical Godunov finite volume [79]. Test cases are given which implement the proposed approaches using Haar wavelet, Symlet wavelets and Coiflet wavelet. Experimental order of ac-

curacy is also formulated for the approach proposed by K.P.Mredula, V.D Pathak, B.M. Shah [54].

Nonlinear Burger equation is solved using wavelet based finite volume in this chapter. The nonlinear equation

$$w_t + [f(w)]_x = \nu w_{xx}, \quad where \qquad f(w) = \frac{\beta w^2}{2} \tag{5.1.17}$$

is utilized. The finite volume method by Mikel [72] for $\beta = 1$ is considered. He integrated equation 5.1.17 with respect to x between $x_{j-\frac{1}{2}}$ and $x_{j+\frac{1}{2}}$ and then rewriting it as,

$$\int_{x_{j-\frac{1}{2}}}^{x_{j+\frac{1}{2}}} w_t dx - [\nu w_x]_{x_{j-\frac{1}{2}}}^{x_{j+\frac{1}{2}}} = -[f(w)]_{x_{j-\frac{1}{2}}}^{x_{j+\frac{1}{2}}} \tag{5.1.18}$$

Now approximating each of the term in equation 5.1.18 as,

$$\int_{x_{j-\frac{1}{2}}}^{x_{j+\frac{1}{2}}} w_t dx \approx \frac{dw}{dt}(x_j, t)h,$$

for h being the step size in x.

$$\begin{aligned} -[\nu w_x]_{x_{j-\frac{1}{2}}}^{x_{j+\frac{1}{2}}} &= \nu[w_x(x_{j-\frac{1}{2}}, t) - w_x(x_{j+\frac{1}{2}}, t)] \\ &\approx \nu[\frac{w(x_j, t) - w(x_{j-1}, t)}{h} - \frac{w(x_{j+1}, t) - w(x_j, t)}{h}] \\ &= -\nu[\frac{w(x_{j+1}, t) - 2w(x_j, t) + w(x_{j-1}, t)}{h}] \end{aligned} \tag{5.1.19}$$

and

$$-[f(w)]_{x_{j-\frac{1}{2}}}^{x_{j+\frac{1}{2}}} = f(w(x_{j-\frac{1}{2}}, t)) - f(w(x_{j+\frac{1}{2}}, t)) \tag{5.1.20}$$

Substituting these into the equation 5.1.18, then dividing by h and taking $W_j(t)$ to be the function $w(x_j, t)$ the system obtained is,

$$\frac{dW_j}{dt} - \nu \frac{W_{j+1} - 2W_j - W_{j-1}}{h^2} = \frac{f(W_{j-\frac{1}{2}}) - f(W_{j+\frac{1}{2}})}{h}.$$

Discretizing the time derivative in forward difference a finite volume discretized form is achieved.

Test cases are solved which compared the solution of the proposed approach with the solution given by Shu- Sen Xie [99], who implemented solution formulation using reproducing kernel function and solution given by Mittal [82], who implemented modified cubic spline method.

Test cases comparing the approaches with results of Asai [7] who used automatic differentiation algorithm and the work of Aksan [29] by quadratic B-Spline functions are shown. This comparison is followed by the analysis of the solution using experimental order of accuracy to justify the validity of the approach.

The proposed approach is implemented to viscous burger equation. The study proved that the error is reduced by introducing the wavelet approximation to finite volume algorithm with various test cases. This is achieved due to the utilization of salient features of conservative property embedded in finite volume approach and localization property of wavelets. The chapter includes description of a function representation by decomposed multi wavelets. Reconstruction of the function is highlighted at a specific resolution. In section 5.2 we begin with discreption of combined approach proposed for solving Burger inviscid equation

5.2 Combined Approach

5.2.1 Burger inviscid equations using Godunov flux

Motivation The burger equation was discovered back in the year 1915 by Bateman [37]. In computational fluid dynamics, the inviscid burger equation plays an important role in development and analysis of many algorithms due to its simple but challenging phenomena[1]. One of the very interesting pattern of series solution for burger equation was due to FAY [84]. It appears that for the same number of freedom, spectral methods do yield better accuracy than finite difference solution especially from the point of view of phase error. However if the problem involves as in sharp variation of the profile then spectral methods do not possess an exponential rate of convergence until the region of rapid change is resolved [30]. The exponential fast convergence is lost as the derivatives are calculated in large regions. The wavelet functions have been utilized for solution of ordinary differential equations, finite element approach and so on during the recent years. Utilizing the finite volume with Godunov flux representation is an added advantage employed in this attempt. With decomposition and reconstruction of solution values at each stage of time step improves the solution.

Burger equation The Burger equations are appearing in most of the approximate theories of flow through a shock wave in viscous fluid, and in study of turbulence. The Burger equation,

$$\frac{\partial w}{\partial t} + w\frac{\partial w}{\partial x} = \upsilon\frac{\partial w^2}{\partial x^2} \tag{5.2.1}$$

is a quasilinear parabolic partial differential equation in which $w(x,t)$ is the dependent variable for most of the fluid mechanics applications with a small valued parameter υ. There is a similarity between the Burgers equation and the Navier-Stokes equations due to the form of the non-linear terms and the occurrence of higher order derivatives with small coefficients in both. The Burgers equation is one of the very few non-linear partial differential equations which can be solved exactly for an arbitrary initial data. For $\upsilon = 0$, the Burgers equation reduces to the momentum equation of gas dynamics as

$$\frac{\partial w}{\partial t} + w\frac{\partial w}{\partial x} = 0 \tag{5.2.2}$$

which is an important test case as considered in this study also.

Core idea The finite volume approach is based on writing the equation in integral form. By considering the homogeneous scalar conservation law that is valid for any arbitrary closed volume on the cartesian mesh [79]. The multi resolution helps in representing any function in $L^2[-1,1]$ as a series of multiwavelets using scaling and dilating function. Here we attempt to bring together the properties of both finite volume along with wavelet representation, for a better solution of the equation with suddenly changing behaviour.

5.3 Review of Approaches used in the algorithm

5.3.1 Multiresolution revisited

A brief discussion of multiresolution in relation to finite volume approach is given. The theory follows from the well known Alpert's multiwavelet algorithm[4]. The interval $[-1, 1]$ is used as one element at level 0 then, divided as two in level 1 and so on. In mathematical sense the interval I_{2j}^{n+1} and I_{2j+1}^{n+1} on level $n+1$ are formed by splitting I_j^n on level n into two equal parts with $n = 0, 1, ..., j = 0, 1, ..., 2^n - 1$. At level n, the domain $[-1, 1]$ is divided into 2^n elements, defined as,

$$I_j^n = [-1 + 2^{-n+1}j, -1 + 2^{-n+1}(j+1)] \quad with, \qquad j = 0, 1, ..., 2^n - 1.$$

Now recalling concepts of multiresolution chapter 2 article 2.1.2, Godunov method chapter 5 section 5.1, wavelets chapter 2 article 2.1.3 and few details from chapter 2, section 2.2, we consider spaces as,

$$V_0^{k+1} = \{f : f \in P^k([-1, 1])\},$$

$$V_1^{k+1} = \{f : f \in P^k[-1, 0) \cup P^k[0, 1]\},$$

$$V_2^{k+1} = \{f : f \in P^k(I_j^2), j = 0, 1, 2, 3\}, ...,$$

$$V_n^{k+1} = \{f : f \in P^k(I_j^n), j = 0, 1, ..., 2^n - 1\}$$

To begin defining multiwavelet in one dimension, the scaling functions was introduced.

The scaling function spaces were defined as above V_n^{k+1} with $P^k(I_j^n)$ being the space of polynomials of degree k, on interval I_j^n with nested property as

$V_0^{k+1} \subset V_1^{k+1} \subset V_2^{k+1} \subset ...V_n^{k+1} \subset ..., \subset L^2[-1,1]$. The space V_n^{k+1} was generated by $2^n(k+1)$ functions which were obtained by dilation and translation of Legendre polynomials, $\phi_0, \phi_1, \phi_2, ..., \phi_k$ as

$$\phi_{lj}^n(x) = 2^{n/2}\phi_l(2^n(x+1) - 2j - 1) \tag{5.3.1}$$

with $\quad l = 0, 1, ..., k \quad$ *and* $\quad j = 0, 1, ..., 2^n - 1.$

The orthogonal projection of an arbitrary function $f \in L^2[-1,1]$ on to $V_n^{k+1}, n \in N$ was given [107] as discussed in details in chapter 2 section 2.2, recalling equation 2.2.9 which is given as,

$$P_n^{k+1} f(x) = \sum_{j=0}^{2^n-1} \sum_{l=0}^{k} s_{l,j}^n \phi_{l,j}^n \tag{5.3.2}$$

where the expansion of the coefficient is given by

$$s_{l,j}^n(i) = \langle f, \phi_{l,j}^n \rangle \tag{5.3.3}$$

The value of the coefficient indicates the location of $f(x)$ at a particular resolution level. This is extended by considering a projection on W_k^n with the multiwavelet bases $\{\psi_{l,j}^n\}$ along with a combined consideration, the function projection is modified as,

$$P_n^{k+1} f(x) = \sum_{l=0}^{p} s_{l,0}^0 \phi_{l,0}^0 + \sum_{n=0}^{N-1} \sum_{j=0}^{2^n-1} \sum_{l=0}^{p} d_{l,j}^n \psi_{l,j}^n(x) \tag{5.3.4}$$

where the detail coefficients were computed as $d_{l,j}^n = \langle f, \psi_{l,j}^n \rangle$.

5.3.2 Decomposition and Reconstruction

We implement the concepts, given by Alpert and Amat [5],[89]. The decomposition due to the nested feature of V_k^n can be represented as,

$$\phi_{l,j}^n(x) = \sum_{m=0}^{2^n-1} \sum_{r=0}^{p} H_{l,r}^m \phi_{r,m}^{n+1}(x) \tag{5.3.5}$$

where $H_{l,r}^m$ are the lowpass quadrature mirror filters. Refer [5] for details.
Similarly for the wavelet functions

$$\psi_{l,j}^n(x) = \sum_{m=0}^{2^n-1} \sum_{r=0}^{p} G_{l,r}^m \phi_{r,m}^{n+1}(x) \tag{5.3.6}$$

with $G_{l,r}^m$ as high pass filters are used. The combined use leads us to the bases decomposition and the inverse which is bases reconstruction.

5.3.3 Finite Volume Godunov Approach

The finite volume approach involves writing the equation 5.2.2 in integral form. With considerations of the homogeneous scalar conservation law that was valid for any arbitrary closed volume on the cartesian mesh the equation in discrete form using Godunov approach was given by [79],

$$w_j^{n+1} = w_j^n - \frac{k}{h}[F(w_j^n, w_{j+1}^n) - F(w_{j-1}^n, w_j^n)] \tag{5.3.7}$$

where a closed volume was represented by a cell i in the domain of x as $[x_{i-\frac{1}{2}}, x_{i+\frac{1}{2}}]$ with time interval $[t^n, t^{n+1}]$ for integration.
Now

$$F(U, V) = \frac{u^{*2}}{2}$$

with $U \geq V$ we obtained,

$$u^* = \begin{cases} U & \frac{U+V}{2} > 0 \\ V & otherwise \end{cases}$$

For $U < V$ we get

$$u^* = \begin{cases} U & U > 0 \\ V & V < 0 \\ 0 & U \leq 0 \leq V \end{cases}$$

Now a step by step formulation of the approach is mentioned in section 5.4,

5.4 Algorithm of the approach used

The proposed Wavelet Finite Volume (WFVM) is described in short by the four steps.

Step 1 The initial condition is decomposed to the wavelet domain and reconstructed to the chosen level of resolution with a specific choice of wavelet.

Step 2 Updating the value for next time step is performed with finite volume formulation by considering the new domain of integration

$$[x_i + \frac{\triangle x}{2}(1 + 2^{-n+1}j), x_i + \frac{\triangle x}{2}(1 + 2^{-n+1}(j+1))],$$

hence evaluation of all the local values within the interval is achieved.

Step 3 Step 1 is repeated for the new value updated at same time step.

Step 4 Then the next updated finite volume step is repeated. The intermediate decomposition and reconstruction of the obtained data improves in tracing the details of change occurring in the solution phenomena and thus proves to be an improved added property. The approach was experimented with the following test cases as given in section 5.5.

5.5 Numerical experiments and discussion

5.5.1 Case 1

The equation 5.2.2 was considered with initial condition $w(x,0) = \begin{cases} 1 & x \leq 0 \\ 0 & x > 0 \end{cases}$

The exact solution is given by $w(x,t) = \begin{cases} 1 & x \leq \frac{t}{2} \\ 0 & x > \frac{t}{2} \end{cases}$ using the method of characteristics. The solution procedure considers x in $[-1,1]$, final time $t = 1$ with step size of 0.01. In WFVM the wavelet considered is Daubechies at level 4 within the interval. The solution comparison for FVM ,WFVM and exact is represented in figure 5.1 with green, blue and red respectively. Figure 5.2 gives the surface plot for exact solution. The table 5.1, gives values for proposed approach with Haar, Symlet and Coiflet wavelet used as basis function.

Table 5.1: The table gives the comparative solution of the proposed method using Haar, Symlets and Coiflet wavelets as basis for case 1.

t	x	Haar	Symlets	Coiflet
0	- 0.4	1	0.99999	1.000002
0.2	- 0.1	1	0.99999	1.000000
0.4	0.1	0.971748	0.971748	0.9717487
0.6	0.3	0.7708705	0.7708705	0.7708705
0.8	0.5	0.3091955	0.30919551	0.3091955
1	1	0	0	0

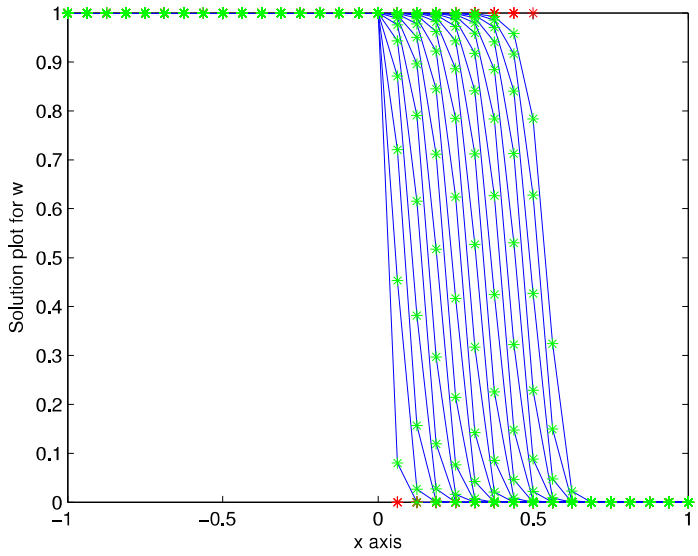

Figure 5.1: Comparative plots for exact in red, FVM in green and WFVM in blue for case 1 with various time levels

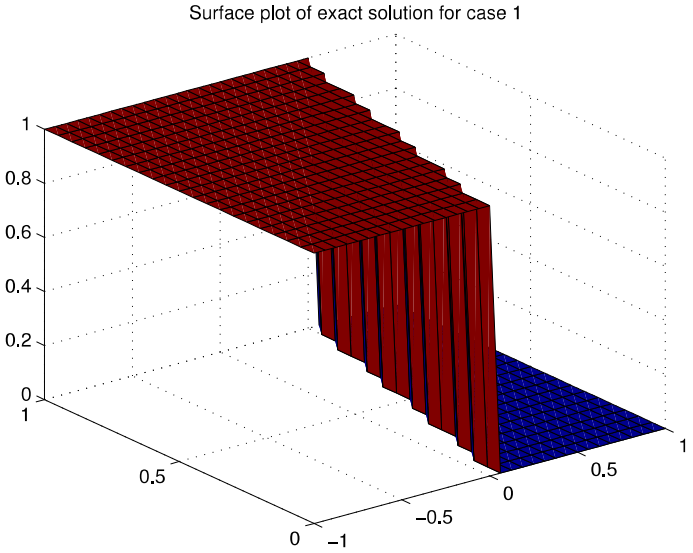

Figure 5.2: The exact solution by method of characteristics for case 1

5.5.2 Case 2

The equation 5.2.2 is considered with initial condition $w(x,0) = \begin{cases} 1 & x < 0 \\ 1-x & 0 \le x \le 1 \\ 0 & x > 1 \end{cases}$

The exact solution is given by $w(x,t) = \begin{cases} 1 & x < t \\ \frac{1-x}{1-t} & t \le x \le 1 \\ 0 & x > 1 \end{cases}$ using the method of characteristics. The solution for wavelet finite volume approach is plotted in figure 5.3 as compared to its exact solution for different time step for x within $[-1, 1]$, final time $t = 1$,with step size of 0.01. Figure 5.4 indicates surface plot for WFVM. The figure 5.3 gives plot for different wavelets chosen as approximating basis to see the performance of the proposed method.

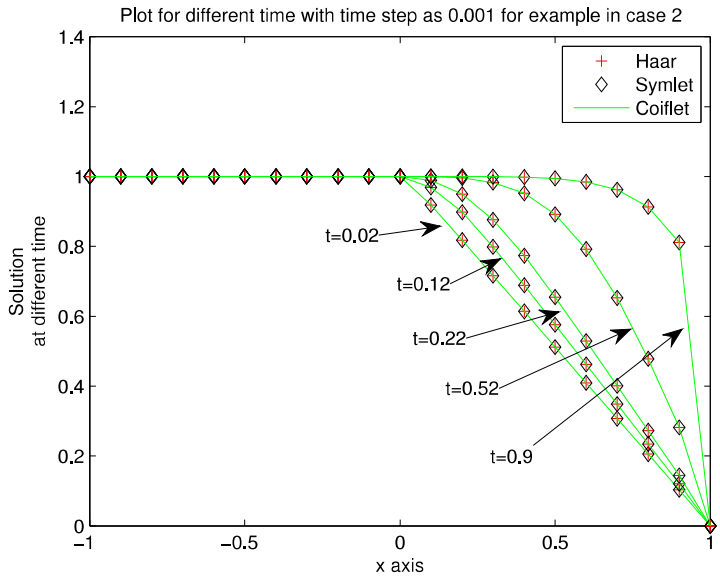

Figure 5.3: Comparative plots for WFVM with different wavelet basis, case 2

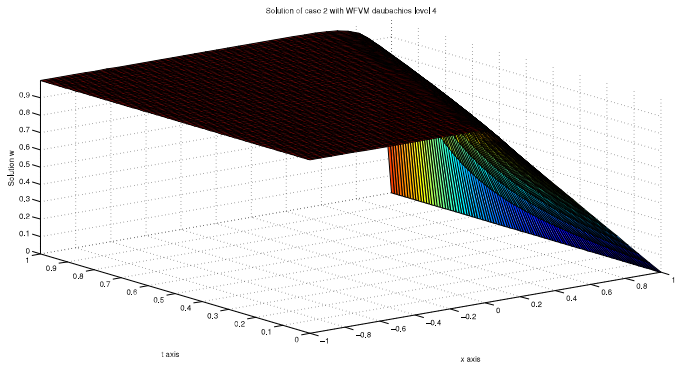

Figure 5.4: Solution by WFVM for case 2 using Daubechies wavelet

5.5.3 Case 3

The equation 5.2.2 with initial condition $w(x,0) = x.$ is solved. The exact solution is given by

$$w(x,t) = \frac{x}{t+1}.$$

In the solution a final time was set to 0.9 with time step 0.01. Coiflet wavelet with level 7 for WFVM was implemented for $x \in [0,1]$.

The plots for a comparative study of FVM in green, WFVM in blue and exact in red, is given in figure 5.5. Figure 5.6 shows WFVM with Coiflet wavelet.

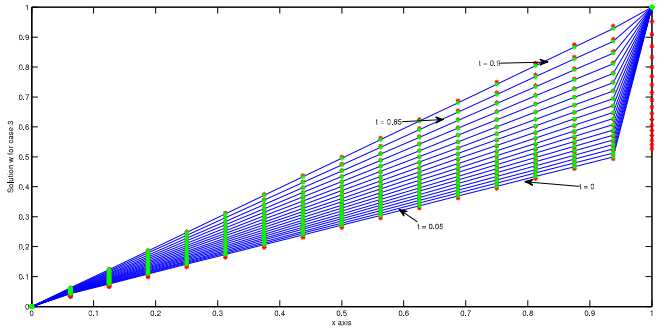

Figure 5.5: Comparative plots for exact in red, FVM in green and WFVM in blue for case 3 with various time levels

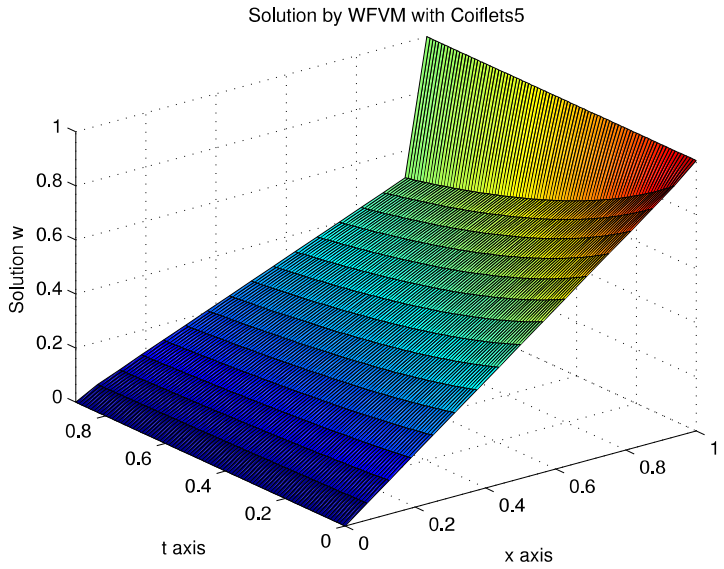

Figure 5.6: Solution of case 3 by WFVM using Coiflet5 level 7

Table 5.2: The experimental order of accuracy is given for case 1

Number of grids	$\varepsilon^{\triangle x}$ Proposed method	EOC
20	8.4709	
40	4.2826	0.9840
80	2.1498	0.9943
160	1.0948	0.9849
320	0.5587	0.9486

5.6 Convergence analysis for the proposed approach

The experimental order of convergence was formulated for the examples computed using the formula,

$$EOC^{\triangle x_1 \triangle x_2} = \frac{\log(\varepsilon^{\triangle x_1}) - \log(\varepsilon^{\triangle x_2})}{\log(\triangle x_1) - \log(\triangle x_2)} \tag{5.6.1}$$

where $\triangle x_1$ and $\triangle x_2$ are the different mesh sizes.

$$\varepsilon^{\triangle x_1} = 100 \frac{\|w^{\triangle x_1} - w^{exact}\|_{L_1}}{\|w^{exact}\|_{L_1}}, \tag{5.6.2}$$

which gives the relative percentage error for the different mesh considered as in equation 5.6.1. w^{exact} indicates the exact solution as a reference value to compute the experimental order of convergence, which is shown to be increasing with increased cell numbers. In table 5.2 for case 1 the EOC for proposed approach is given which indicates an accelerated value of EOC, converging to one.

5.7 Observations

The study gives a modified approach with combination of two phenomena and the error is observed in terms of root mean square error between the exact and WFVM. It was observed that the results are quiet comparable with case 1, the error was noted between 0.0139 to 0.1445 . The case 2 showed a reading of error to be between 0.004 and 0.0553 with case 3 it was noted as between 0.0051 and 0.1152. The results were agreeable with the existing procedures of FVM but the benefit observed was the flexibility to analyse the solution due to multi resolution which was an added advantage due to the fusion of approaches. The benefit of finite volume and wavelet

were fully utilized due to the adaptability of the approach to different resolutions as per the requirement for observing the sudden change in pattern of the solution. The comparitive study with different wavelets like Haar, Symlet, Coiflet suggest that the choice of basis depends on the type of example considered for better precision. The experimental order of convergence is also analyzed for the proposed method with case 1 which indicates that the convergence level is approaching 1 faster with an increase of grids.

The study also indicates that selection of various wavelet families as basis for the proposed approach is depending on the case handled, the performance of the varied choices do not alter the solution to a large extent.

5.8 Viscous Burger equation using finite volume approach

A new algorithm was implemented which combines the finite volume and wavelet approximation to bring together the salient features of both the approaches for obtaining numerical solution of nonlinear viscous burger equation under various initial and boundary conditions. The approach was based on approximating the values using wavelet and then it was combined with finite volume formulation. It uses the localization property of wavelet basis. The root mean square error is studied to establish the improvement in the solution as compared to the classical approaches. Plots and tables indicate the significance of the algorithm discussed.

5.8.1 Motivation

The concept of numerical approximation for solution of a partial differential equation, is widely implemented in many applications. Various approaches like wavelet based finite difference [23],[56],[52], finite element[5], finite volume applicaton in shallow water problem [38], their combinations like discontinuous galerikin in shock tube, blast wave problem and Shu Osher problem as in [107], [51] have been used by the researchers.

We consider the classical non linear burger equation

$$\frac{\partial w}{\partial t} + \beta w \frac{\partial w}{\partial x} - \nu \frac{\partial^2 w}{\partial^2 x} = 0, \tag{5.8.1}$$

$$a \leq x \leq b, \quad t > 0$$

with initial and boundary conditions as $w(x,0) = f_0(x),\ a \leq x \leq b$ and $w(a,t) = g_0(t)$ and $w(b,t) = g_1(t)$, $t \in [0,T]$ where $\nu > 0$ is a small parameter known as the kinematic viscosity and β is some positive constant.
The Burger's equation is the simplest nonlinear model equation for diffusive waves in fluid dynamics. Burger's equation arises in many physical problems including one-dimensional turbulence, sound waves in a viscous medium, shock waves in a viscous medium, waves in fluid filled in viscous elastic tubes, and magneto-hydrodynamic waves in a medium with finite electrical conductivity.
Many numerical solutions have been proposed namely B-spline collocation [18], [44], Galerikin finite element approach [2]. We compare our results with [82], [29],[99], [7].

The method proposed here for solving nonlinear burger equation combines the wavelet based approach and the parabolic method in a novel pattern to bring to-

gether the benefits of both the approaches.

5.8.2 Discretization

The governing equation 5.8.1 is discretized using the finite volume method [72]. We rewrite the equation 5.1.17,

$$w_t + [f(w)]_x = \nu w_{xx}, \quad where \qquad f(w) = \frac{\beta w^2}{2} \tag{5.8.2}$$

Now by integrating equation 5.8.2 with respect to x between $x_{j-\frac{1}{2}}$ and $x_{j+\frac{1}{2}}$, equation 5.8.2 is converted into following discretized form,

$$w_j^{n+1} = w_j^n + k(\nu \frac{w_{j+1}^n - 2w_j^n + w_{j-1}^n}{h^2} + \frac{f[w_{j+\frac{1}{2}}^n] - f[w_{j-\frac{1}{2}}^n]}{h}) \tag{5.8.3}$$

where $f[w_{j\pm\frac{1}{2}}^n]$ is the average of $f[w_j^n]$ and $f[w_{j\pm1}^n]$. k and h indicates the time and space step size respectively. Utilizing the wavelet approximation similar to burger inviscid equation as in previous section 5.3.1. The following algorithm is proposed

5.9 Algorithm proposed for viscid Burger equation

Algorithm combines the features of discretization and mutiscaling, to obtain a more reliable approach. The underlying idea is as follows:

- The time and space is discretized with $\triangle t$ and $\triangle x$ as per the requirement of the example. Initialization of the viscosity parameter is done.

- The function that represents the solution as per the initial condition is decomposed using multiscale decomposition by equation 5.3.4
- To go to the next time step we use finite volume frame work equation 5.8.3 in article 5.8.2, and then again wavelet decomposition is performed according to equation 5.3.4.
- The above step is repeated upto time T.
- Solution at all time step is represented in terms of a matrix..

5.10 Numerical experiments and discussion

In order to justify the implementation and adaptability of the algorithm three examples are discussed in details as

5.10.1 Example 1

The nonlinear Burger equation

$$\frac{\partial w}{\partial t} + \beta w \frac{\partial w}{\partial x} - \nu \frac{\partial^2 w}{\partial^2 x} \quad = 0, \tag{5.10.1}$$

$t > 0$ for $\beta = 1$ with initial condition $w(x, 0) = -\sin \pi x$, $\nu = \frac{10^{-2}}{\pi}$ and $x \in [-\pi, \pi]$ is solved using the proposed approach with time step $\frac{1}{300\pi}$. The plot is given in figure 5.7. The analytic solution is given in [13] with surface plot figure 5.8. Figure 5.9 shows the surface plot of proposed approach. Figure 5.10 gives the root mean square error plot for both classical parabolic and wavelet based proposed approach.

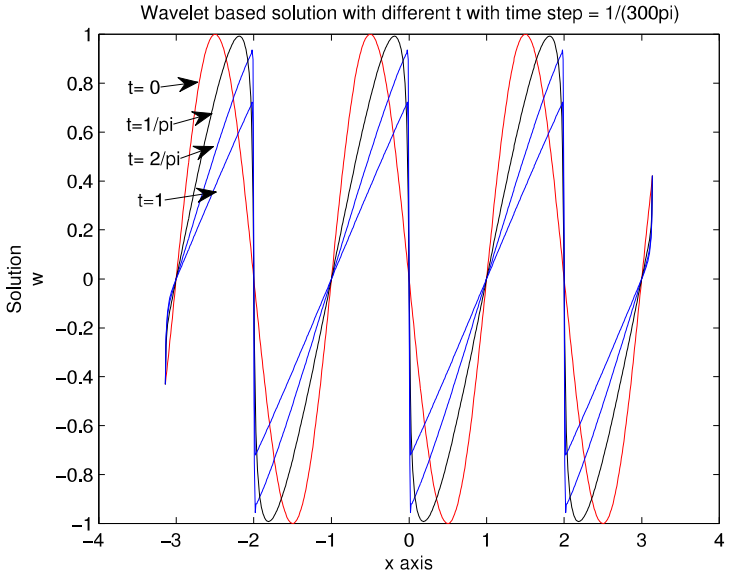

Figure 5.7: Wavelet based solution plot for the example 1

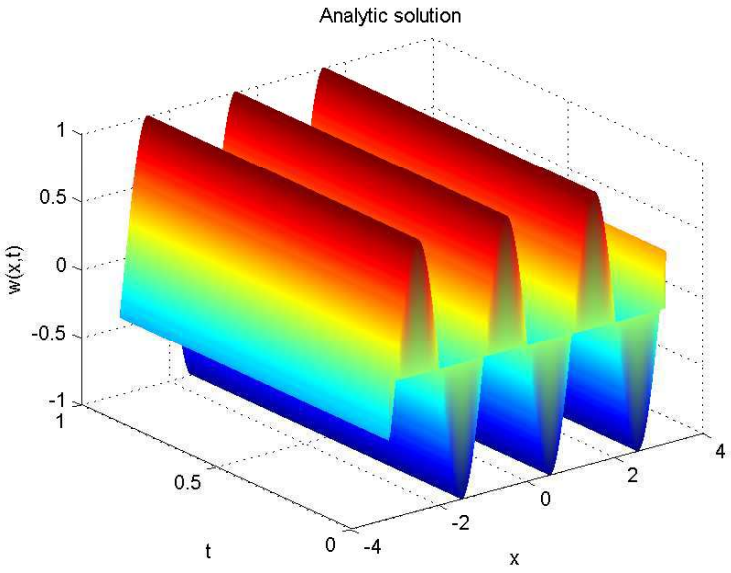

Figure 5.8: Analytic solution plot for example 1

5.10.2 Example 2

Considering the same equation 5.10.1 with $\beta = 1$ for $x \in [0, 1.2]$ with initial condition $w(x,1) = \frac{x}{1+\exp(\frac{1}{4\nu}(x^2-\frac{1}{4}))}$ with boundary conditions $w(0,t) = 0$ and $w(1.2,t) = 0$.

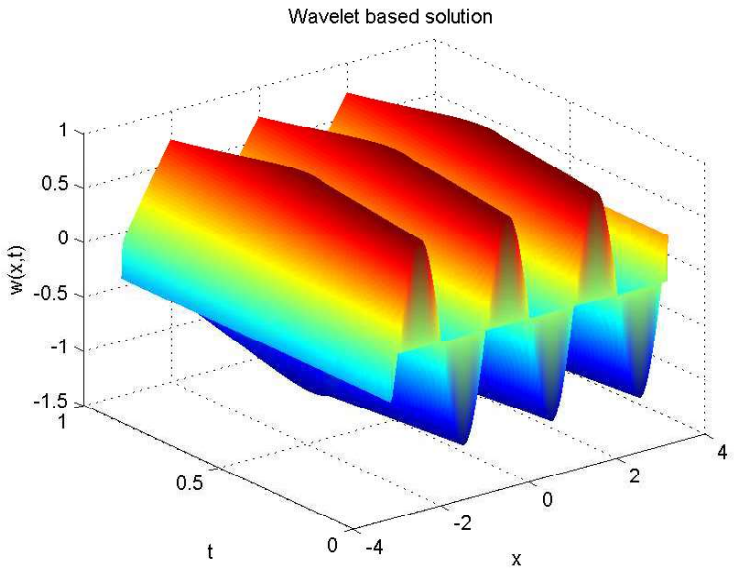

Figure 5.9: Wavelet based solution plot for example 1

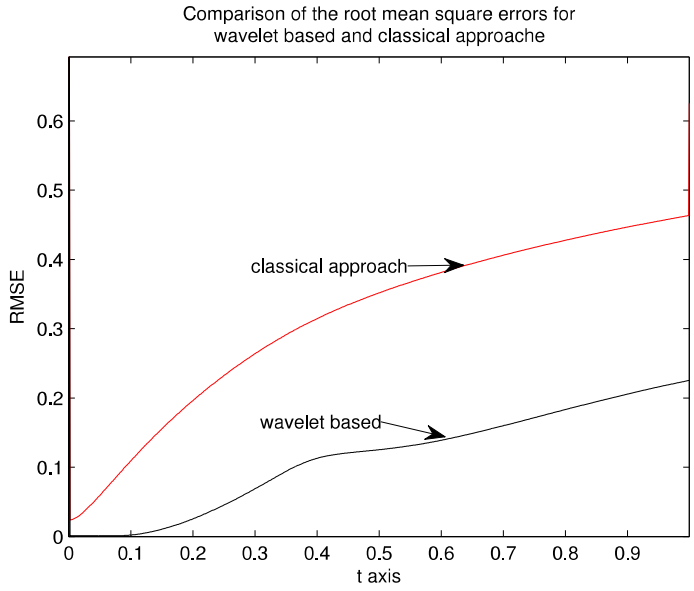

Figure 5.10: Root mean square error of classical parabolic and wavelet based parabolic solution with analytic value example 1.

The example is solved for $\nu = 0.005$, the step length of x as 0.01 and for time as 0.001. to obtain figure 5.11.

Table 5.3: The experimental order of convergence as per equation 5.6.1 for example 1.

No of cells	$\varepsilon^{\triangle x}$	EOC
5	29.9071	
10	29.5381	0.0179
16	13.9055	1.6031
32	12.8645	0.1122

The analytic solution is given by

$$w(x,t) = \frac{\frac{x}{t}}{1 + (\frac{t}{t_0})^{\frac{1}{2}} \exp(\frac{x^2}{4\nu t})}$$

with $t \geq 1$ and $t_0 = \frac{1}{8\nu}$.

The results obtained are compared with results obtained by [82], [99] with courser x grids in table 5.4.

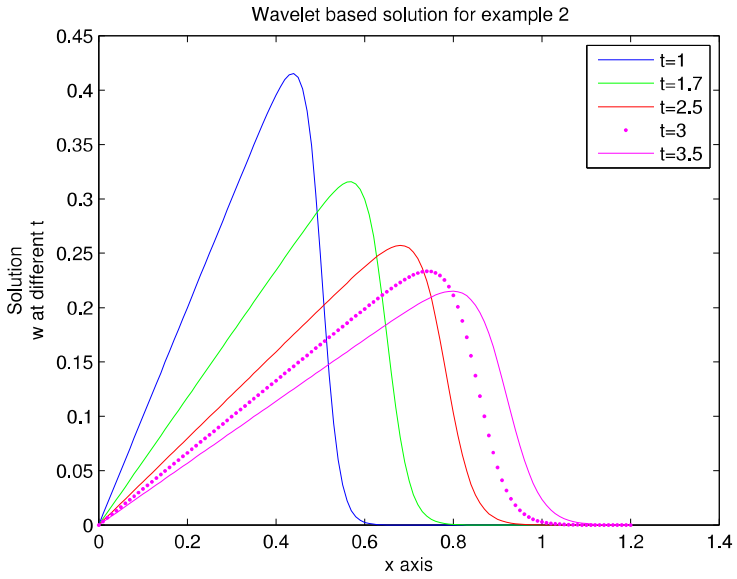

Figure 5.11: Solution for $\nu = 0.005$, $\triangle t = 0.001$ between 0 and 1 for $t \leq 3.6$ for example 2.

Table 5.4: Comparison of solution using numerical and analytic solution for $\triangle x = 0.01, \triangle t = 0.001, \nu = 0.005$ for example 2.

x	t	Shu [99] $\triangle t = 0.01$, $\triangle x = 0.0001$	Mittal [82] $\triangle t = 0.001$ $\triangle x = 0.005$	Proposed $\triangle t = 0.001$ $\triangle x = 0.05$	Proposed $\triangle t = 0.001$, $\triangle x = 0.01$	Analytic Solution
0.2	1.7	0.1176565	0.1176452	0.1176093	0.1173452	0.1176452
	2.5	0.0800527	0.079999	0.0799701	0.0797990	0.079999
	3.0	0.0667147	0.066665	0.066641	0.0664658	0.0666658
	3.5	0.0571820	0.05714	0.057122	0.0571422	0.0571422
0.4	1.7	0.2332111	0.235169	0.234525	0.235169	0.2351677
	2.5	0.1591735	0.159977	0.159964	0.1599214	0.1599769
	3.0	0.1328314	0.133321	0.133289	0.1332738	0.1333209
	3.5	0.1139606	0.114278	0.1142459	0.1142380	0.1142779
0.6	1.7	0.2940048	0295857	0.2816436	0.2964038	0.2959097
	2.5	0.2347876	0238129	0.2422683	0.2382074	0.2381207
	3.0	0.1973222	0.199483	0.1997065	0.1994634	0.1994805
	3.5	0.1697753	0.171225	0.1712523	0.1711861	0.1712242
0.8	1.7	0.0008917	0.000638	0.0019488	0.0006381	0.0006465
	2.5	0.1103866	0.102132	0.0931274	0.1016980	0.1020957
	3.0	0.2088346	0.208803	0.2021463	0.2088032	0.2088359
	3.5	0.2119293	0.214593	0.222798	0.2145838	0.2145869

5.10.3 Example 3

The equation 5.10.1 is solved with $\beta = 1$ with time step 0.001, $w(x, 0) = 4x(1 - x)$. The boundary conditions $w(0, t) = 0$ and $w(1, t) = 0$ with x step length as 0.025 and $\nu = 0.01$ is considered.

The analytic solution is given by

$$w(x,t) = \frac{2\pi\nu \sum_{n=1}^{\infty} a_n \exp^{-n^2\pi^2\nu t}\, n \sin n\pi x}{a_0 + \sum_{n=1}^{\infty} a_n \exp^{-n^2\pi^2\nu t}\, n \cos n\pi x} \tag{5.10.2}$$

Table 5.6 gives the comparative results for our approach with results in [29], [7], and they are quiet satisfactory.

Table 5.5: The experimental order of convergence according to equation 5.6.1 for Example 2 at $\triangle t = 0.001$

No of cells	$\varepsilon^{\triangle x}$ for FVM	$\varepsilon^{\triangle x}$ for proposed method	EOC FVM	EOC Proposed Method
10	17.7418	17.7211		
20	5.1822	5.1550	1.7755	1.7814
40	1.2608	1.2236	2.0392	2.0748
80	0.2932	0.2625	2.1044	2.2207

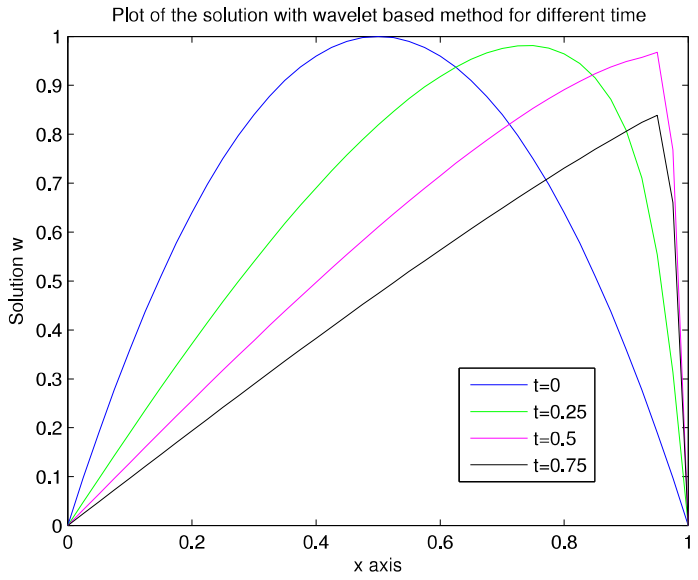

Figure 5.12: Solution for $\triangle x = 0.025$, $\triangle t = 0.001$, $t \leq 3$ and $\nu = 0.01$. for example 3

5.11 Convergence analysis for the proposed approach

The experimental order of convergence is formulated for the examples computed using the formula given in equation 5.6.1. which gives the relative percentage error for the different mesh considered as in table 5.3 and table 5.5. w^{exact} indicates the exact solution as a reference value to compute the experimental order of convergence,

Table 5.6: Comparison of solution using numerical and analytic solution for $\triangle x = 0.025, \triangle t = 0.001$ for proposed method, $\nu = 0.01$ for example 3.

x	t	Asai [7] $\triangle x = 0.0125$ $\triangle t = 0.0001$	Aksan[29] $\triangle x = 0.025$ $\triangle t = 0.0001$	Proposed $\triangle x = 0.025$ $\triangle t = 0.001$	Analytic Solution
0.25	0.4	0.36232	0.36225	0.362356	0.3622
	0.6	0.28209	0.28199	0.2820722	0.28204
	0.8	0.23049	0.23039	0.2304514	0.23045
	1.0	0.19472	0.19463	0.1946725	0.19469
	3.0	0.07614	0.07611	0.07611154	0.07613
0.50	0.4	0.68380	0.68371	0.6839751	0.68368
	0.6	0.54840	0.54835	0.548424	0.54832
	0.8	0.45377	0.45374	0.453692	0.45371
	1.0	0.38572	0.38568	0.3856223	0.38568
	3.0	0.15219	0.15216	0.152134	0.15218
0.75	0.4	0.92101	0.92047	0.9219043	0.92050
	0.6	0.78324	0.78302	0.783568	0.78299
	0.8	0.66285	0.66276	0.662885	0.66272
	1.0	0.56940	0.56936	0.5693176	0.56932
	3.0	0.22786	0.22773	0.2277426	0.22774

which is shown to be increasing with increased cell numbers. In table 5.5 for example 2 the comparison of EOC for both classical finite volume and proposed approach is given which indicates an accelerated value of EOC with the classical approach.

5.12 Observations

In this chapter, we developed a wavelet based finite volume method for solving nonlinear Burgers equation using Daubechies wavelet as basis functions. In the present method we combined the features of localization due to wavelet approximation and the salient feature of finite volume which utilizes conservation laws within cell interface.

The flux conservation defined in average sense over each cell contributes in the improvement of accuracy. This method is tested on three test problems, and the root mean square error plot figure 5.10 for example 1 clearly indicates the reduced error. The solution by our approach as shown for example 2 in section 5.10, given in table 5.4, by using courser x grid $\triangle x = 0.05$ and $\triangle x = 0.01$ compares very well and gives even closer to the analytical solution as compared to the results obtained by other researchers [99], [18].

It is interesting to note in example 3 given in section 5.10, that we have considered 10 times larger time step than other researchers as in [7],[29], given in table 5.6 which helps in obtaining the solution at the desired time faster, with comparable solution.